

Dynamic simulator and model predictive control of an integrated solar combined cycle plant

Ponce, Carolina V.; Saez, Doris; Bordons, Carlos; Nunez Vicencio, Alfredo

DOI

[10.1016/j.energy.2016.04.129](https://doi.org/10.1016/j.energy.2016.04.129)

Publication date

2016

Document Version

Accepted author manuscript

Published in

Energy

Citation (APA)

Ponce, C. V., Saez, D., Bordons, C., & Nunez Vicencio, A. (2016). Dynamic simulator and model predictive control of an integrated solar combined cycle plant. *Energy*, 109(August), 974-986.
<https://doi.org/10.1016/j.energy.2016.04.129>

Important note

To cite this publication, please use the final published version (if applicable).
Please check the document version above.

Copyright

Other than for strictly personal use, it is not permitted to download, forward or distribute the text or part of it, without the consent of the author(s) and/or copyright holder(s), unless the work is under an open content license such as Creative Commons.

Takedown policy

Please contact us and provide details if you believe this document breaches copyrights.
We will remove access to the work immediately and investigate your claim.

1 Dynamic Simulator and Model Predictive Control of 2 an Integrated Solar Combined Cycle Plant

3 Carolina V. Ponce ^a, Doris Sáez ^b, Carlos Bordons ^c, Alfredo Núñez ^d

4 ^a University of La Serena, La Serena, Chile. cponce@userena.cl

5 ^b University of Chile, Santiago, Chile. dsaez@ing.uchile.cl

6 ^c University of Seville, Seville, Spain. bordons@us.es

7 ^d Delft University of Technology, Delft, The Netherlands. a.a.nunezvicencio@tudelft.nl

8

9 **Abstract**

10 This paper presents the design and evaluation of a dynamic simulator for an integrated solar
11 combined cycle (ISCC) plant. The design of the simulator is based on the
12 phenomenological equations for both a combined cycle plant and a solar plant. The
13 simulator incorporates a regulatory control strategy based on proportional-integral (PI)
14 controllers and was developed in the MATLAB/Simulink® environment. A model
15 predictive control (MPC) strategy established at a supervisory level is presented. The intent
16 of the strategy is to regulate the steam pressure of the superheater of the ISCC plant. The
17 combined use of the simulator and the supervisory control strategy allows for the
18 quantification of the reduction in fuel consumption that can be achieved when integrated
19 solar collectors are used in a combined cycle plant. The ISCC plant simulator is suitable for
20 designing, evaluating and testing control strategies and for planning the integration of solar
21 and combined cycle plants.

22 **Keywords**

23 Integrated solar combined cycle power plant, solar-collector-based steam generator,
24 combined cycle power plant, supervisory model predictive control.

25

26 **Highlights**

- 27 ➤ Simulator for planning and control of integrated solar combined cycle plants;
- 28 ➤ Analysis of steam support provided by a solar plant;
- 29 ➤ Savings of fuel supplied to the furnace;
- 30 ➤ Supervisory model predictive control allows reduction of fuel consumption in the
- 31 auxiliary burner.

32

33 **Nomenclature**

ARIX	Auto-Regressive Integrated with Exogenous input	I_{wF}	Indicator of fuel used in kg/s
CC	Combined Cycle	\overline{IJ}	Global index for the total objective function
HP	High Pressure	\overline{IJ}_{cr}	Global index for the regulatory term
HRSG	Heat Recovery Steam Generation	\overline{IJ}_{cf}	Global index for the fuel cost
HTF	Heat Transfer Fluid	J	Objective function
ISCC	Integrated Solar Combined Cycle	J_{cr}	Objective function regulatory term
MPC	Model Predictive Control	J_{cf}	Objective function fuel-cost term
SSG	Solar Steam Generator	t_{sim}	Simulation time s
$f(L)$	Function depending on drum shape		

34 **Nomenclature and values**

Symbol	Quantity	Value
C_{pa}	Specific heat of oil $J/(kg \cdot K)$	3795.5
C_v	Specific heat of steam from the drum $J/(kg \cdot K)$	5000
C_f	Fuel cost per flow unit $US\$/ (kg/s)$	798
C_{gm}	Specific heat of steam from the SSG $J/(kg \cdot K)$	5000
C_{st}	Heat capacitance of the superheater tubes $J/(kg \cdot K)$	481.4
C_{ps}	Specific heat of steam at constant pressure $J/(kg \cdot K)$	2330
f_s	Superheater friction coefficient m^{-4}	2615
h_s	Specific enthalpy of superheated steam J/kg	3.3117×10^6
h_{ref}	Reference steam enthalpy J/kg	3.32×10^6
h_v	Specific enthalpy of saturated steam (drum) J/kg	2.7977×10^6
h_a	Attemperator water specific enthalpy J/kg	5.5217×10^6
h_e	Feed water specific enthalpy	5.6217×10^5

h_f	Specific enthalpy of evaporation J/kg	1.987×10^6
h_{gm}	Specific enthalpy of SSG steam J/kg	2.8087×10^6
h_w	Specific enthalpy of liquid water J/kg	variable
h_{wv}	Specific enthalpy of saturated water J/kg	variable
K_{ec}	Coefficient $kg/(K*s)$	0.6124
k_s	Experimental heat transfer coefficient $J/(kg*K)$	4.37×10^4
k_i	Integral constant	2×10^{-8}
k_p	Proportional constant	3×10^{-6}
L^*	Reference drum level m	4.1425
M_s	Mass of the superheater tubes kg	1.04×10^4
m_a	Oil mass flow from the storage tank of the solar plant kg/s	3.6491
m_{d1}	Drum liquid mass kg	3817.6
p_{eg}	SSG inlet water mass flow pressure Pa	2.9×10^6
p_G	Furnace gas pressure Pa	1.013×10^5
p_s	Superheated steam pressure Pa	4.5251×10^6
p_s^r	External steam pressure set point Pa	4.5251×10^6
p_s^*	Steam pressure set point Pa	4.5251×10^6
\hat{p}_s	Steam pressure step-ahead prediction	variable
p_v	Steam drum pressure Pa	4.5417×10^6
p_{vgm}	SSG inlet water mass flow pressure $mm\ hg$	21.75×10^3
P_G	Gas turbine power MW	34
P_s	Steam turbine power MW	11
P_G^*	Gas turbine power set point MW	34
P_s^*	Steam turbine power set point MW	34
Q_{gs}	Heat supplied to the superheater (from the furnace) J/s	3.0117×10^6
Q_s	Heat transferred to the steam J/s	5.6105×10^6
Q_a	Heat supplied to the oil from solar radiation J/s	2.7003×10^6
Q_{gm}	Heat supplied to the SSG steam J/s	2.7003×10^6
R_s	Ideal gas constant for water $Pa \cdot m^3 / kg \cdot ^\circ K$	461.5
T_a	Inlet temperature of the oil from the storage tank of the solar plant K	568
T_w	Water temperature in the drum K	526.76
T_g	Outlet temperature of the superheated steam K	variable

T_{gm}	Steam temperature of the SSG K	505.017
T_v	Saturated steam temperature in the drum K	505
T_{st}	Superheater metal tube temperature K	735.3078
T_s	Superheated steam temperature K	717.72
T_t	Superheater inlet steam temperature K	526.52
T_{ref}	Reference steam temperature K	723.15
T_0	Saturated steam temperature at pipe pressure K	505
v_{dow}	Volumetric liquid flow rate through downcomer m^3/s	0.71556
V	Drum volume m^3	9.253
V_L	Drum liquid volume m^3	4.8425
V_s	Superheater volume m^3	8.462
V_v	Vapor volume m^3	4.4105
w_{gm}	Steam mass flow from the SSG kg/s	1.2
w_{gm}^*	Reference steam mass flow from the SSG kg/s	1.2
w_{eg}	Inlet mass flow of liquid water kg/s	1.2
w_F	Fuel mass flow kg/s	variable
w_T	Total superheated steam mass flow kg/s	13.2
w_v	Steam mass flow from the drum to the superheater kg/s	12
w_e	Water flow from the economizer kg/s	12
w_{ec}	Liquid mass evaporation from the drum	0
w_d	Water mass flow to the downcomer kg/s	564.11
w_r	Liquid vapor mixture mass flow kg/s	564.11
w_s	Steam mass flow out of the superheater kg/s	10.8
w_A	Air steam mass flow kg/s	64.093
w_{at}	Attemperator water mass flow kg/s	0
α, β, λ	Weighting parameters	$10^8, 1, 10^2$
τ_g	Empirical time constant of flow s	1
ρ_T	Total superheated steam density kg/m^3	13.662
ρ_s	Superheated steam density kg/m^3	13.662
ρ_v	Saturated steam density kg/m^3	22.763
ρ_w	Drum water density kg/m^3	788.34
x	Steam quality	variable
xsI	Dummy variable J/m^3	4.524×10^7

35 **1. Introduction**

36 The construction of integrated solar combined cycle (ISCC) power plants has provided a
37 remarkable technological contribution toward sustainable power generation [7]. In addition, the
38 integrated construction of such plants is highly effective because combined cycle (CC) plants
39 can operate more efficiently than other types of plants. An ISCC power plant features three
40 main components: a CC thermal power plant, a distributed collector field and a solar steam
41 generator. The solar steam generator is the component that connects the solar collector plant to
42 the combined cycle plant and allows for the transfer of energy between them. Fig. 1 shows a
43 diagram of an ISCC plant consisting of a high-temperature gas turbine, a steam turbine and a
44 solar collector plant. Steam for the turbine is provided by two sources: the boiler and the solar
45 field [1]. Preheated feed water is extracted from the high-pressure preheater, evaporated and
46 slightly superheated in the solar steam generator. Then, it goes to the boiler, and together with
47 the steam from the conventional evaporator, it is superheated to reach the steam temperature.

48

49 The first electric power generation plant to integrate a combined cycle plant with a distributed
50 solar collector (i.e., an ISCC plant) is located in HassiR'mel, Algeria [6]. The plant features a
51 150 MW combined cycle generator with a solar share of 30 MW_{el} net (or 35 MW_{el} gross). The
52 cost to build the plant was 425 million USD. The solar plant consists of a field of distributed
53 solar collectors; thermal oil (the heat transfer fluid, HTF) circulates through a tube at a
54 temperature of 393°C at the outlet of the field. The largest ISCC plant in the world is located in
55 Ain Beni Mathar, Morocco. Egypt [13] and Iran [14] also have ISCC plants in which hot oil is
56 used as the transfer fluid. Italy, through its Archimedes Project, operates a 750 MW plant with
57 5 MW of solar energy; in this plant, a molten salt eutectic mixture (60% NaNO₃ and 40%

58 KNO₃) is used as HTF. Due to the high solidification temperature of the molten salts (around
59 290 °C), other options like the direct production of steam in the solar collector or the use of
60 gaseous fluids like CO₂ as HTF are being studied [11]. Florida, USA, also possesses several
61 ISCC plants, with 74 MW of solar energy. To the best of our knowledge, the most recently
62 constructed plant of this type is Agua Prieta II in Mexico (470 MW with a solar contribution of
63 14 MW). Similar plants are also being constructed in Australia and India [1]. The plants located
64 in Morocco, Algeria and Egypt cost 416 million Euros, 315 million Euros and 150 million
65 Euros, respectively, to construct. Nezammahalleh et al. [17] have reported that the levelized
66 energy cost of the Iranian ISCC plant is 76.45 USD/MWhe. Given that the ISCC technology is
67 relatively new, various technical and economic studies, such as those by Horn et al. [13] and
68 Hosseini et al. [14], have been conducted to evaluate the feasibility of such plants in various
69 geographical locations. The factors that have been evaluated include thermal efficiency and
70 capacity, environmental considerations, investment, and fuel cost. It has been concluded that
71 operating an ISCC plant is more commercially viable than operating a single solar power plant
72 and that ISCC plants are capable of providing environmental and economic benefits for electric
73 power generation. Amelio et al. [2] evaluate the performance of an innovative ISCC plant,
74 considering linear parabolic collectors where the heat transfer fluid is the same oxidant air that
75 is introduced into the combustion chamber. With this configuration, the net average year
76 efficiency is 60.9% against the 51.4% of a reference combined cycle plant without solar
77 integration.

78 A thermodynamic evaluation of the ISCC plant located in Yazd, Iran, was performed by
79 Baghernejad and Yaghoubi [4], [5]. The energy and exergy of the solar field and the ISCC
80 plant were analyzed, and the thermoeconomics required to minimize the cost of investment in

81 equipment and the cost of exergy in the ISCC plant were considered. Al-Sulaiman [2] also
82 conducted an exergy analysis of a solar collector plant, including the analysis of an ISCC plant
83 that produces steam via the Rankine cycle. Several refrigerants were examined, and among the
84 combined cycles that were examined, the combined cycle known as R134a demonstrated the
85 best exergetic performance, with a maximum exergetic efficiency of 26%. Kelly et al. [15]
86 searched for the optimal method of transferring solar thermal energy from a combined cycle
87 plant to produce electrical energy. Among the three investigated alternatives, the most efficient
88 method was to remove the feed water from the heat recovery steam generator, downstream
89 from the second-stage economizer (with the highest temperature), thereby producing high-
90 pressure saturated steam, and then to return the steam to the heat recovery steam generator to
91 be superheated and reheated by the gas turbine exhaust gases. Cau et al. [11] analyzed the
92 behavior of an ISCC plant in which the heat transfer fluid is CO₂. The results indicated that the
93 energy conversion efficiency of such plants is slightly better than that of systems based on
94 steam cycles and is very similar to that of systems that generate electricity directly from steam.
95 Nezammahalleh et al. [17] performed a conceptual design and technical/economic evaluation of
96 a combined cycle plant with integrated solar collectors for the direct generation of electricity
97 from steam. This technology was compared with the ISCC plant in Iran, in which oil is used as
98 the HTF, and with a solar power plant. The authors concluded that the cost of the ISCC plant,
99 which generates electricity directly from steam, is lower than that of the other two systems.

100

101 Nowadays, different ways to integrate a combined cycle-plant with solar power plants are
102 possible. One of those ways is by using solar tower power plants as in Spelling et al. [23]. In
103 [23], a thermo-economic optimization is performed, minimizing the investment costs and the
104 levelized electricity costs by using an evolutionary multi-objective optimization algorithm. An

105 efficiency around 18-24% can be reach, depending on the initial investment. Lambert et al. [16]
106 analyse the energy cost of CO₂ capture for a natural gas combined cycle plant, and the
107 integration with a solar tower system. Different cases are studied, including the exhaust gas
108 recirculation and the pre-combustion case that uses the exhaust gas recirculation with the
109 capture being realized after the compression stage of the gas turbine. It was found that addition
110 of solar energy reduces the total energy costs.

111

112 Because of the importance ISCC plants have attained, it necessary to develop simulators that
113 model these plants to satisfy various objectives, such as the evaluation of control strategies,
114 optimization, or planning. Cau et al. [11] used the software GateCycle® for the evaluation of
115 ISCC plants. GateCycle® enables the design of CC plants, fossil boiler plants, cogeneration
116 systems, combined heat and power plants, advanced cycle gas turbines, and many other energy
117 systems. The software can be used for evaluation, design, remodeling, re-powering, and
118 acceptance testing. However, this software does not include models of solar collectors;
119 therefore, the authors first developed a model for solar collector plants and then evaluated a CC
120 plant using GateCycle®. Aftzoglou [1] performed a study of an ISCC plant from the
121 thermodynamic perspective based on the principle of overheating. For this study, the simulator
122 CycleTempo was used. CycleTempo is a tool for the thermodynamic analysis and optimization
123 of systems designed for the production of electricity, heat and refrigeration. It should be noted
124 that both the GateCycle® software and the simulator proposed by Aftzoglou [1] are steady state
125 simulators whose purpose is the design of ISCC plants. By contrast, the simulator proposed in
126 this paper is a dynamic simulator for the design and dimensioning of ISCC plants, the study
127 and design of control strategies, and dynamic optimization. Thus, this paper presents a new
128 and, to the best of our knowledge, unique contribution to ISCC plant design because no other

129 dynamic simulator of this type has yet been reported in the literature.

130

131 **2. Plant Description**

132 The ISCC power plant analyzed in this study corresponds to the integration of a CC plant with
133 both a supplementary fired boiler and a distributed solar collector plant. The idea is to replace
134 some fraction of the steam produced by the supplementary fired boiler with steam produced in
135 a steam generator that uses oil heated in a solar collector plant. The integration of the solar
136 plant into the CC plant was achieved following the study by Kelly et al. [15].

137

138 **2.1 Combined Cycle Power Plants**

139 In a CC power plant, a gas turbine and a steam turbine are used to generate electrical power. The
140 exhaust gas from the gas turbine is used to generate steam in the boiler. The boiler extracts heat
141 from the exhaust gas to increase the temperature and pressure of the steam. In a CC plant with a
142 supplementary fired boiler, in addition to the heat recovered from the exhaust gas, an additional
143 firing is provided to the boiler, thereby increasing the amount of steam produced. The electrical
144 efficiency may be lower than that of the standard configuration (without a supplementary firing
145 to the boiler), but there is additional flexibility in that the boiler may be supplied with a different
146 type of fuel from that of the turbine [18].

147

148 **2.2 Solar Collector Plants**

149 The solar power plant considered in this paper is a solar thermal plant featuring parabolic
150 collectors. The parameters considered in the simulator emulate the operation of the real plant

151 located in the desert of Tabernas, Southern Spain. The plant consists of a field of 480
152 distributed solar collectors grouped into 20 rows and 10 parallel loops. Each loop has a length
153 of 172 m, and the total open surface area is 2672 m². The primary objective of this type of solar
154 plant, namely, one based on a distributed collector field, is to collect solar energy by heating oil
155 that is passing through the field. The field is also provided with a tracking system, which causes
156 the mirrors to revolve around an axis parallel to the pipe, thereby enabling the collectors to
157 reduce the angle between the rays of the sun and a vector normal to the aperture of the collector
158 (angle of incidence). Cold inlet oil is extracted from the bottom of the storage tank and passed
159 through the field by a pump located at the field inlet. This fluid is heated and then returned to
160 the storage tank. The type of oil used in this plant is Santotherm 55. The operating temperature
161 range is -25 °C to 290 °C. In many parts of the world, especially Europe, Solutia markets
162 Therminol 55 HTFs under the name of either Santotherm 55 or Gilotherm 55. This fluid has a
163 low thermal conductivity, and its density is highly dependent on temperature. One storage tank
164 can be used to contain both hot and cold oil. The tank used in this field has a capacity of 140
165 m³, which allows for the storage of 2.3 thermal MWh; it has an inlet temperature of
166 approximately 210 °C and an outlet temperature of approximately 290 °C [8].

167

168 **3. The ISCC Dynamic Simulator**

169 A dynamic simulator for a combined cycle power plant with integrated solar collectors (i.e., an
170 ISCC plant) was developed using MATLAB/Simulink®. The design is based on a simulator for
171 a solar collector plant, ACUREX [8], and on the combined cycle plant simulator developed by
172 Sáez et al. [22], which is based on the phenomenological equations presented by Ordys et al.
173 [17]. This simulator is useful for studying the behavior of variables relevant to an ISCC plant,

174 for comparing the dynamics of an ISCC plant with those of a CC plant and for ISCC plant
 175 design. Among the relevant variables to consider are the fuel flow from the furnace, the drum
 176 level, the steam pressure in the superheater and the furnace gas pressure. The simulator is also
 177 designed to assess the reduction in the fuel consumption of the furnace relative to the fuel
 178 consumption of CC plants. The simulator was developed for a 45 MW combined cycle thermal
 179 power plant consisting of a boiler, a $P_s=11$ MW steam turbine and a $P_g=34$ MW gas turbine.
 180 The available simulator for the ACUREX solar plant is able to deliver a peak thermal power of
 181 1.2 MW. Various representative examples of ISCC plants can generate higher power. In this
 182 paper, the primary objective of the scale test simulator is to reproduce the most relevant
 183 phenomenological processes of ISCC plants. For the integration of a solar plant and a solar
 184 steam generator (SSG) into a combined cycle plant, it is necessary to add certain equipment,
 185 such as pumps and valves, in addition to adapting the equations that describe the dynamics of
 186 the CC plant superheater. The equations that describe the dynamics of the drum do not change.
 187 According to Ordys et al. [18], the equations for the drum are as follows:

$$188 \quad w_e + (1-x)w_r - w_d - w_{ec} = \frac{d}{dt}(m_{d1}) \quad (1)$$

$$189 \quad \frac{m_{d1}}{\rho_w} = f(L) \quad L = f^{-1}\left(\frac{m_{d1}}{\rho_w}\right)$$

$$190 \quad V_L = f(L) = \pi r^2 L \quad (2)$$

$$191 \quad w_d = v_{dow} \rho_w \quad (3)$$

$$192 \quad w_e h_e + (1-x)w_r h_{rv} = w_d h_w + w_{ec} h_v + \frac{d}{dt}(m_{d1} h_w) \quad (4)$$

193
$$w_{ec} + xw_r - w_v = \frac{d}{dt}(V_v \rho_v) \quad (5)$$

194
$$w_{ec} = K_{ec}(T_w - T_v) \quad (6)$$

195
$$V_v = V - V_l \quad (7)$$

196 where equation (1) represents the liquid mass balance, (2) the drum liquid level, (3) the
197 downcomer mass flow, (4) the liquid heat balance, (5) the steam mass balance, (6) the
198 evaporation dynamics and (7) the vapor volume.

199

200 In designing the dynamic simulator for an ISCC plant, the following assumptions were
201 adopted:

- 202 - The solar plant has its own field controller that keeps the outlet oil set point temperature
203 for changing weather conditions. This controller adjusts the oil flow in the solar field in
204 order to reject the disturbances caused by the variation of solar radiation along the day and
205 changes in the return inlet oil temperature. The solar plant has a storage tank which
206 provides energy from which the oil that passes to the solar steam generator is extracted and
207 decouples both parts of the plant. So, although the oil flow is not fixed (since it is
208 continually manipulated by the solar field controller), the solar support can be considered
209 constant. Therefore, when the solar field is in operation, the thermal energy supplied by the
210 storage tank is kept at its nominal value.
- 211 - From the previous assumption, it follows that the temperature of the oil inlet to the solar
212 steam generator can be held constant during day-to-day planning operations.
- 213 - The water mass flow from the feed water to the drum in the CC plant is the same as the
214 water mass flow from the feed water to the drum in the ISCC plant.

- 215 - The gas turbine and the steam turbine are similar in both the CC and ISCC simulators. The
216 only difference is the source of energy used to heat the steam.
- 217 - Basic PI controllers are considered because they are typically implemented efficiently in
218 real plants for the control of steam pressure, drum level, furnace gas pressure, superheated
219 steam temperature, exhaust gas temperature, NO_x concentration in exhaust gas and turbine
220 mechanical power. Thus, the PI control loops of the ISCC plant simulator are similar to
221 those of the CC plant simulator. A feedforward controller is incorporated for the feed water
222 supplied to the SSG.

223

224 **3.1 Design of the Solar Steam Generator Simulator**

225 An SSG uses oil that was previously heated in a solar collector plant and then stored in an
226 energy storage tank. The heat of the oil is transferred to liquid water, producing steam that then
227 passes into the combined cycle plant. The oil from the solar plant has a certain temperature T_a
228 and a given mass flow m_a . The inlet liquid water in the SSG has an enthalpy h_w and a
229 temperature T_w , but as it flows through the heat exchanger and the water is heated to the
230 saturated steam temperature corresponding to the inlet flow pressure p_{eg} , saturated steam with a
231 steam enthalpy of h_{gm} is produced. Subsequently, the output emits a steam flow that
232 corresponds to w_{gm} and a heat flow of Q_{gm} . Fig. 2 shows a schematic diagram of the heat
233 interchange process between the oil from the storage tank of the solar plant and the water from
234 the heat recovery steam generator (HRSG) of the CC plant.

235

236 As described by Dersch et al. [12], Price et al. [19] and Kelly et al. [15], the SSG was designed
237 by considering an inlet water flow of 10% of the water flow injected into the drum of the CC
238 plant.

239

240 The characteristics of the oil from the ACUREX solar collectors were also considered, i.e., the
241 specific heat, temperature and mass flow of the oil. Fig. 3 presents a diagram that depicts the
242 inputs and outputs of the SSG simulator. The inlet water mass flow pressure p_{eg} is derived from
243 the pump used to increase the water flow pressure from the feed water (Fig. 1), and saturated
244 steam is obtained in the SSG. The equations that describe the SSG are as follows:

$$245 \quad C_{pa} = 1820 + 3.478T_a \quad (8)$$

$$246 \quad T_0 = \frac{3816.4}{18.304 - \ln(p_{vgm})} + 46.13 \quad (9)$$

$$247 \quad h_{gm} = -1.8934 \cdot 10^6 + 4.1404 \cdot 10^4 T_0 - 148.7585 \cdot T_0^2 + 0.2471 \cdot T_0^3 - 1.5519 \cdot 10^{-4} \cdot T_0^4 \quad (10)$$

$$248 \quad Q_a = m_a C_{pa} (T_a - T_0) \quad (11)$$

$$249 \quad Q_{gm} = -Q_a \quad (12)$$

$$250 \quad \frac{d}{dt} w_{gm} = (w_{eg} - w_{gm}) / \tau_g \quad (13)$$

251 where (8) to (12) are algebraic equations and (13) a differential equation. Equation (8)
252 describes the specific heat of the oil Therminol 55 as a function of its temperature. Other
253 properties of the oil, such as its thermal conductivity, dynamic viscosity and Prandlt number,
254 also depend on the temperature [9], [10]. Equation (9) is the steam saturation temperature as
255 described by Reid et al. [20]. Saturated steam is produced at a high temperature and then enters
256 the superheater. Equation (10) represents the enthalpy of saturated steam as a function of the

257 steam temperature, as suggested in a study conducted by Reynolds [21]. In Equation (11), the
258 heat transferred to the oil from solar radiation is a function of the oil temperature and the steam
259 saturation temperature. Equation (12) is a heat balance, heat received by the steam in the heat
260 exchanger is equal to the heat provided by the oil; thus, heat losses are negligible. The steam
261 flow at the outlet of the steam generator (w_{gm}) can be obtained using equation (13), where the
262 speed of the steam flow equals the difference between the inflow to and outflow from the
263 exchanger divided by a time constant (τ_g).

264

265 In the SSG simulation process, the values of T_a and m_a from the solar plant are read. w_{eg} and p_{eg}
266 are also read, where the first variable is derived from the feed water and the second is obtained
267 from the pump installed at the outlet of the feed water. The initial SSG conditions and
268 parameters are defined. Algebraic equations (8) to (12) are solved. Then, w_{gm} is obtained via
269 equation (13) using w_{eg} and τ_g . The values obtained for h_{gm} , Q_{gm} , T_o and w_{gm} are applied to the
270 superheater. This loop is repeated at each sampling time step. The attemperator is part of the
271 superheater. The inflow to the superheater is w_T , whereas w_s corresponds to the outflow of the
272 superheater, which is the steam at the input to the turbine. Both are shown in Fig. 3.

273

274 In Fig. 3 the control loop in the drum regulates its level by opening or closing the valve when
275 the level is lower or higher than the reference. The control loop in the steam turbine keeps the
276 turbine power near the power reference demand by changing the flow of steam coming from
277 the superheater. If power demand increases, the valve is opened to increase the mass flow of
278 superheated steam. If the power demand decreases, the valve is closed to reduce the steam
279 flow. The water supply of the steam generator also has a control loop and it works similarly to

280 the control level of the drum. The reference value in this case corresponds to the amount of
281 liquid water that could be converted into steam in the SSV.

282

283 3.2 Design of the ISCC Simulator

284 As previously stated, the design of the ISCC simulator considered in this study is based on the
285 CC simulator developed by Sáez et al. [22] with the integration of a solar plant [8]. The same
286 equipment is considered in the design of both the CC and solar plants, with the only difference
287 being the energy source that heats a fraction of the steam going to the superheater. In general,
288 the models were developed using the basic principles of conservation of energy, mass and
289 momentum. The SSG output steam, w_{gm} , is injected into the boiler of the combined cycle plant
290 in the superheater stage. The injected steam is added to the steam from the drum w_v . All steam
291 present in the superheater, w_T , is heated to a superheated state. Finally, the superheated steam,
292 w_s , is injected into the steam turbine in the high-pressure section (HP). The equations that
293 describe the dynamics of the superheater are as follows:

294

$$295 \quad p_v - p_s = \frac{w_T^2}{\rho_T} f_s \quad (14)$$

$$296 \quad Q_s = k_s w_T^{0.8} (T_{st} - T_s) \quad (15)$$

$$297 \quad \begin{aligned} \Delta h &= C_{ps} (T_s - T_{ref}) \\ T_s &= (h_s - h_{ref}) / C_{ps} + T_{ref} \end{aligned} \quad (16)$$

$$298 \quad p_s = R_s \rho_s T_s \quad (17)$$

$$299 \quad w_v C_v (T_t - T_v) = w_{gm} C_{gm} (T_{gm} - T_t) \quad (18)$$

$$300 \quad T_t = \frac{w_v T_v + w_{gm} T_{gm}}{w_v + w_{gm}} \quad (19)$$

$$301 \quad w_v - w_s + w_{gm} + w_{at} = V_s \frac{d}{dt}(\rho_s) \quad (20)$$

$$302 \quad Q_{gs} + Q_{gm} = Q_s + M_s C_{st} \frac{d}{dt}(T_{st}) \quad (21)$$

$$303 \quad Q_s + w_v h_v + w_{gm} h_{gm} = w_s h_s - (h_a - h_f) \cdot w_{at} + V_s \frac{d}{dt}(\rho_s h_s) \quad (22)$$

304 where (14) to (19) are algebraic equations, and (20) to (22) are differential equations. The
 305 losses due to friction that are generated in the pipelines where the total steam (w_T) passes to the
 306 steam turbine are estimated based on momentum balance in equation (14). Equation (15) was
 307 empirically deduced and describes the heat transfer between the metal (pipelines) and the
 308 steam, considering turbulent flow. As in equation (14), the total steam is considered in the
 309 relation. The superheated steam temperature is obtained using equation (16), where the
 310 variation in the enthalpy between a temperature T_s and the reference temperature T_{ref} is
 311 calculated under the assumption of ideal conditions. Assuming an ideal gas model, where R_s is
 312 the universal gas constant, the superheated steam pressure is obtained in equation (17). The
 313 total steam generated in the superheater originates from two sources, the SSG and the exhaust
 314 gas turbine. The temperatures of these two sources are different. A mixture of both flows must
 315 be considered in the energy balance, as in equation (18). Under the assumption of a constant
 316 heat capacity $C_v \approx C_{gm}$, the temperature of the inlet steam that arrives at the superheater is
 317 obtain using equation (19). Through mass balance, the total steam in the superheater is
 318 obtained in equation (20). The inflow is equal to the outflow of the superheater; thus, losses are
 319 negligible. Note that in (20), an average behavior of density along the pipe is considered. This

320 assumption could be relaxed and in a future work the steam density changes along the pipe
321 could be modelled. In equation (21) is the superheater heat balance. The heat that is transferred
322 to the steam, according to the furnace model, incurs losses in the pipelines through which the
323 steam flows (final term of the equation). The heat balance equation (22) for steam includes the
324 energy provided by the steam from the SSG; therefore, this balance equation is different from
325 that presented by Sáez et al. [22].

326

327 In the first step of the superheater simulation process, w_a , w_s , p_v , Q_{gs} , h_v , h_o , w_{gm} , h_{gm} , Q_{gm} , T_{gm} ,
328 and T_o are measured. The superheater parameters are defined, and the initial conditions for xsI ,
329 h_s and p_s are provided. Then, xsI is calculated. Algebraic equations (14) to (19) are solved.
330 Then, differential equations (20) to (22) are solved. P_s , T_s , h_s , and ρ_s are sent to the steam
331 turbine. The loop is repeated at each sampling time. Other routines used in the simulator have
332 already been implemented and reported by Ordys et al. [18] and Sáez et al. [22]. At the
333 beginning of the paper, the nomenclature and the variable ranges used in the simulators are
334 specified.

335

336 **4. Model Predictive Control at the Supervisory Level for an ISCC Plant**

337 A Model Predictive Control (MPC) strategy at the supervisory level for ISCC plants was
338 designed. The output of the supervisory level scheme is used as a set point for the steam
339 pressure in the boiler at the regulatory level. Fig. 4 illustrates a scheme for such a control
340 strategy. The external set point p_s^* is constant and corresponds to the steady-state superheater
341 steam pressure.

342

343 The output variables of the boiler are the furnace pressure of the gases (p_G), the temperature of
 344 the steam at the outlet of the boiler (T_S) and the level of the drum of the CC plant (L). These
 345 variables are controlled using PI controllers at the regulatory level. For the supervisory control
 346 strategy, the input is p_s and the output is p_s^r .

347

348 **4.1 System Identification**

349 For the supervisory-level model, an ARIX (Auto-Regressive Integrated with Exogenous input)
 350 model was established for the outlet pressure of the steam flow of the superheater, p_s , as a
 351 function of the fuel flow of the afterburner, w_F . For the design of the supervisory-level control
 352 scheme, a data set was obtained from the simulator by varying the reference pressure (p_s^r) and
 353 adding pseudorandom binary noise. The reference values were varied between 3.5×10^6 and
 354 5.4×10^6 Pa. Furthermore, a model for the regulatory-level PI controllers was obtained for the
 355 fuel flow w_F as a function of p_s^r . The sampling time of this model is $t_m = 10$ s, and its structure
 356 is as follows:

$$357 \quad A(z^{-1})p_s(t) = B(z^{-1})w_F(t) + \frac{e(t)}{\Delta} \quad (23)$$

358 where $e(t)$ is white noise; z^{-1} is the delay operator, $z^{-1}y(t) = y(t-1)$; $\Delta = 1 - z^{-1}$; and the
 359 polynomials $A(z^{-1})$ and $B(z^{-1})$ are of 13th order:

$$360 \quad A(z^{-1}) = 1 + a_1z^{-1} + a_2z^{-2} + a_3z^{-3} + a_4z^{-4} + a_5z^{-5} + a_6z^{-6} + a_7z^{-7} + a_8z^{-8} +$$

$$a_9z^{-9} + a_{10}z^{-10} + a_{11}z^{-11} + a_{12}z^{-12} + a_{13}z^{-13}$$

$$361 \quad B(z^{-1}) = b_1z^{-1} + b_2z^{-2} + b_3z^{-3} + b_4z^{-4} + b_5z^{-5} + b_6z^{-6} + b_7z^{-7} +$$

$$b_8z^{-8} + b_9z^{-9} + b_{10}z^{-10} + b_{11}z^{-11} + b_{12}z^{-12} + b_{13}z^{-13}$$

362 This model was obtained by evaluating the RMS errors between the actual values and the
 363 values obtained using ARIX models of different orders (structure optimization). The model
 364 with the lowest RMS error was thus selected. To calculate the control variable w_F , a PI
 365 controller is considered as follows:

$$366 \quad w_F(s) = \left(K_p + \frac{K_i}{s} \right) (p_s^r(s) - p_s(s)) \quad (24)$$

367 where $K_p = 3 \times 10^{-6}$, $K_i = 2 \times 10^{-8}$, $p_s^r(s)$ is the reference pressure for the superheated steam, and
 368 $p_s(s)$ is the real pressure of the superheated steam.

369

370 4.2 Objective Function

371 The objective function used for the supervisory MPC strategy is given by

$$372 \quad J = J_{cr} + \lambda J_{cf} \quad (25)$$

$$373 \quad J_{cr} = \alpha \sum_{k=1}^N (\hat{p}_s(t+k) - p_s^*)^2 + \beta \sum_{k=1}^N \Delta w_F^2(t+k-1) \quad (26)$$

$$374 \quad J_{cf} = \sum_{k=1}^N C_f w_F(t+k-1) \quad (27)$$

375 and the following operational constraints over the fuel flow are included:

$$376 \quad 10 \leq w_F(t+k-1) \leq 14.5, \quad k = 1, \dots, N \quad (28)$$

377 where $\hat{p}_s(t+k)$ is the k-step-ahead prediction for the reference pressure, $w_F(t+k-1)$ is the fuel
 378 flow and $\Delta w_F(t+k-1)$ is the control effort at instant $t+k-1$. The first term in equation (25) is a

379 regulatory term, whereas the second term optimizes the fuel costs. In equation (26), the second
380 term accounts for the optimization of the control effort together with the tracking error. In
381 equation (27), C_f is the fuel cost per flow unit in US\$/(kg/s). The minimum and maximum
382 values defined in constraint equation (28) are chosen from [18] and they correspond to the
383 constraints over the start-up and the maximum admissible fuel flow of the CC plant. Finally,
384 the decision variable p_s^r is obtained by minimizing the objective function of equation (25),
385 considering the corresponding constraints and using the PI controller model given by equation
386 (28).

387

388 4.3 Parameter Tuning of the Supervisory MPC Strategy

389 In equations (25) and (26), the weights (λ , α , β) are obtained from the design of the objective
390 function. Each of these weights represents the relative importance of the function by which it is
391 multiplied. To optimize these variables, we adopted a simulation-based approach in which, for
392 a fixed value of $\beta=1$, different values of α and λ were tested over the entire simulation period.
393 A broad range of values were evaluated. Based on global performance statistics, the optimal
394 tuning parameters were obtained; in this case, these parameters were found to be $\alpha=10^8$ and
395 $\lambda=10^2$. To consider the performance of the system over the entire simulation period t_{sim} , each
396 pair of parameters was assessed based on global statistics:

$$397 \quad \overline{J} = \frac{1}{t_{sim}} \sum_{k=1}^{t_{sim}} J(k) = \frac{1}{t_{sim}} \sum_{k=1}^{t_{sim}} (J_{Cr}(k) + \lambda J_{Cf}(k)) \quad (29)$$

$$398 \quad \overline{J}_{Cr} = \frac{1}{t_{sim}} \sum_{k=1}^{t_{sim}} J_{Cr}(k) \quad (30)$$

399
$$\overline{J}_{cf} = \frac{1}{t_{sim}} \sum_{k=1}^{t_{sim}} J_{cf}(k) \quad (31)$$

400 where equation (29) is the global performance index for the total objective function, equation
401 (30) is the global performance index for the regulatory term, and equation (31) is the global
402 index for the fuel cost. Using these parameters, good overall controller performance was
403 achieved, with a reasonable trade-off between the tracking error on the pressure of the steam in
404 the boiler and the reference value given by the supervisory MPC scheme, while maintaining
405 minimal burning of the fuel at the auxiliary burner.

406

407 **4.4 Performance Index**

408 To compare the fuel consumption between a CC plant and an ISCC plant, the amount of fuel
409 saved is defined as the amount of fuel consumed by the CC plant minus the amount of fuel
410 consumed by the ISCC plant; under the assumption that the amount of fuel used by the CC
411 plant corresponds to 100%, the percent reduction in the amount of fuel supplied to the furnace
412 is calculated as the amount of fuel consumed by the CC plant minus the amount of fuel
413 consumed by the ISCC plant, divided the amount of fuel consumed by the CC and multiplied
414 by 100. To compare the performance of the ISCC plant with and without the implementation of
415 the supervisory MPC strategy, the following global indicator of the fuel used at the auxiliary
416 burner was defined:

417
$$I_{wF} = \frac{1}{t_{sim}} \sum_{k=1}^{t_{sim}} w_F(k) \quad (32)$$

418

419

420 **5. Simulation Results**

421 **5.1 Comparison of the ISCC Plant with the CC Plant**

422 To validate the behavior of the ISCC plant simulator, several simulations were performed, as
423 many with the ISCC simulator as with the CC simulator. The results obtained for different
424 cases and using different variables were compared. The behaviors of both the controlled and
425 manipulated variables of the boiler were studied. The controlled variables that were studied
426 included the steam pressure in the superheater, p_s ; the drum level, L ; the pressure of the gases in
427 the furnace, p_G ; and the temperature of the superheated steam in the superheater, T_s . The
428 manipulated variables that were studied included the flow of fuel from the auxiliary burner of
429 the furnace, w_F ; the water flow from the economizer, w_e ; the air flow from the auxiliary burner
430 of the furnace, w_A ; and the mass flow of water from the attemperator, w_{at} . Manipulated
431 variables are also known as decision variables. The purpose was to optimize those variables
432 such that the ISCC plant exhibited both good tracking performance and reduced fuel costs. Two
433 cases are presented: one in which a supervisory controller was used, and one in which a PI
434 controller was used. To illustrate the behavior of the controllers, a step-function change in the
435 reference value of the steam pressure was applied, and the dynamic response is presented in
436 Fig. 5. After 40 s approx., the transient responses are observed for both controllers achieving
437 the new set-point. The overshoot is lower with the supervisory controller compared with the PI
438 control strategy.

439

440 A downward step of 10% was applied to the set point of the gas turbine power (P_G^*) and to the
441 set point of the steam turbine power (P_s^*). This downward step was applied in three different
442 cases: first for the CC plant simulator, then for the ISCC plant simulator with 10% steam

443 support from the SSG and, finally, for the ISCC plant simulator with 20% solar support. The
444 objective of these simulations was to vary the behavior of the controlled and manipulated
445 variables pertaining to the furnace before the addition of steam support from the SSG and, in
446 particular, to verify that the flow of fuel, w_F , diminishes when solar plant support is added. Fig.
447 6 shows the results obtained for the controlled variables of the boiler when P_s^* (the steam
448 turbine power set point) was varied in both simulations. Fig. 7 shows the results obtained for
449 the manipulated variables when P_s^* was varied. As we expected, the variables return to the set-
450 points for all cases. A slight increase is observed for steam pressure of the superheater when the
451 20% steam support is considered. The fuel flow as well as air flow decrease when the steam
452 support increase, because less steam from the HRSG is required. On the contrary, water flow
453 from the economizer increases. Fig. 8 shows the results obtained for the controlled variables
454 when P_G^* (the gas turbine power set point) was varied in both simulations. When a step change
455 is applied to the gas turbine power, the variable will return to its set-point because the same
456 local control strategy is considered for both CC and ISCC cases. Fig. 9 shows the results
457 obtained for the manipulated variables in this latter case. The controlled variables return to the
458 set-points for all cases. The fuel flow is reduced when the steam support increased, because less
459 steam produced by HRSG is required.

460

461 Figs. 7 and 9 show that the ISCC plant demonstrates lower fuel consumption, w_F . This result
462 holds whether the variation in power demand occurs in the gas turbine or in the steam turbine.
463 The fuel consumption decreases as the steam contribution from the solar plant increases. Figs. 6
464 and 8 also illustrate that the water level of the drum, L , in the ISCC plant remains constant as
465 the steam supply from SSG varies (for variations of 10% or 20%). The pressure of the steam in

466 the superheater does not change as the extent of solar support increases from 10% to 20%. The
467 gas pressure of the furnace, p_G , and the temperature of the superheated steam, T_s , remain
468 constant as the support from the solar plant increases. The reason why these variables remain
469 nearly constant is the different control loops that operate for each of the variables.

470 Table 1 shows the percentage fuel savings achieved when using an ISCC plant compared with a
471 CC plant, i.e., the fuel savings realized by introducing the steam from a solar plant. This
472 calculation was performed for solar contributions of 10%, 15% and 20%, which corresponds to
473 possible changes of available solar contribution along the year. It is evident that the amount of
474 fuel saved increases with increasing solar support, as expected. The fact that the simulator can
475 compute these quantities may be very useful for the design and optimal operation of ISCC
476 plants.

477 Fig. 10 shows the behavior of the heat flow being transferred from the furnace to the
478 superheater (Q_{gs}) when the ISCC plant remains constant as the steam supply from SSG varies
479 (for variations of 10% or 20%) as well as the steam power set-point diminishes at $t = 50$ s. It
480 appears that the heat support provided by the furnace to the superheater that is required to
481 produce the same power diminishes upon the addition of support provided by the solar plant.
482 When the heat support from the solar plant is bigger, less heat support provided by the furnace
483 to the superheater is required. Therefore, in this case, the furnace uses less fuel to produce the
484 same amount of power. It appears that the heat support provided by the furnace to the
485 superheater that is required to produce the same power diminishes upon the addition of support
486 provided by the solar plant. When the heat support from the solar plant is bigger, less heat
487 support provided by the furnace to the superheater is required. Therefore, in this case, the
488 furnace uses less fuel to produce the same amount of power.

489 **5.2 Comparison of ISCC Plant Performance with Supervisory MPC and** 490 **PI Control Strategies**

491 The fuel consumption savings achieved using supervisory MPC and PI control strategies were
492 calculated. Table 2 compares the simulation-based results obtained using the index given by
493 equation (32), corresponding to the amount of fuel consumed over a simulation period of 500 s.
494 Considering that an ISCC plant operates over 12 consecutive hours, because the simulator
495 design assumes that the oil is extracted from the storage tank, the savings in fuel consumption
496 amounts to $\Delta w_F = 1754$ kg. Over one year of operation, this savings would be approximately
497 $\Delta w_F = 1,280,361.6$ kg. In February 2014, the price of natural gas in Chile was 1.44 US\$/kg;
498 thus, such a savings would amount to approximately 1,843,721 US\$/year. These results
499 demonstrate the relevance of implementing a proper supervisory strategy, particularly when
500 comparing a supervisory MPC strategy with the conventional PI strategy at the regulatory level.
501 For the same power demand, fuel consumption can be better optimized using the MPC-based
502 strategy than with a PI controller alone. It is considered that the plant operates for 24 hours
503 because the simulator assumes that the oil is extracted from the storage tank, which allows the
504 oil temperature to remain constant. We assumed that the SSG has a well-sized storage that is
505 used for ensuring the supply of 24-hours.

506 The following is an analysis of the effects of changes in the reference powers for the gas
507 turbine and the steam turbine that allows for a better understanding of how fuel consumption
508 varies in each of these cases. Two types of variations in the reference powers of the steam
509 turbine and the gas turbine were considered. First, the reference power was decreased by 10%
510 and then increased by 10%. This test was performed for both the supervisory MPC strategy and
511 the regulatory-level PI controller. Fig. 11 shows the evolutions of the steam pressure with the

512 supervisory MPC strategy (p_s supervisory), with the PI controller (p_s PI) and with the reference
513 pressure (p_s^r) for a decrease of 10% in the reference power of the steam turbine and in that of
514 the gas turbine. The figure shows that the steam pressure response p_s exhibits a lower overshoot
515 in the case of the supervisory MPC strategy for a decrease in the reference power of the steam
516 turbine. With respect to a change in the reference power of the gas turbine, the difference
517 between the responses of the two controllers is minimal, indicating that both strategies can
518 successfully push the pressure of the steam flow toward its reference value. Fig. 12 shows the
519 evolution of the manipulated variable w_F (fuel flow). It can be observed that when the power
520 demand of the steam turbine (P_s^*) decreases, fuel consumption also decreases. This occurs for
521 both control strategies, but the decrease is greater in the case of a supervisory MPC strategy.
522 That is, under the same operating conditions, less fuel is used when the plant employs a
523 predictive control strategy. When the reference power decreases in the gas turbine, an increase
524 in fuel flow occurs for both strategies, but in the case of the supervisory MPC strategy, the
525 increase in fuel flow is lower.

526 Fig. 13 shows the evolution of the steam pressure in the superheater when an increase in the
527 reference power of the steam turbine or the gas turbine occurs for both control strategies. As in
528 the previous cases, the results demonstrate that both controllers are able to maintain the steam
529 pressure responses within similar ranges. When the power of the gas turbine increases, less
530 overshoot is observed for the supervisory control strategy. When the power of the steam turbine
531 increases, the steam pressure response is similar for both controllers, but the response with the
532 supervisory MPC strategy is faster. Fig. 14 shows the fuel consumption incurred with the
533 supervisory MPC strategy and the regulatory-level PI controller strategy when the reference
534 powers of the steam turbine and gas turbine are increased. When the power of the steam turbine

535 is increased, an increase in fuel consumption is observed in the auxiliary burner; however, in
536 the case of the system controlled with a supervisory MPC scheme, this increase is much lower.
537 Moreover, when the reference power of the gas turbine increases, the fuel consumption of the
538 afterburner decreases, exhibiting a greater reduction in the case of the supervisory-MPC-
539 controlled system. Thus, the fuel consumption is greater when PI control at the regulatory level
540 is applied.

541 Table 3 summarizes the savings in fuel consumption achieved by changing the reference values
542 of the steam and gas turbines. The index I_{WF} was calculated using equation (32). Additionally,
543 the differences in fuel consumption between the two control strategies are presented in terms of
544 net values and percentages. In Table 3, a negative sign (-) represents a decrease in the set point
545 and a positive sign (+) represents an increase in the set point.

546

547 **6. Conclusions**

548 A dynamic simulator for a combined cycle plant with integrated solar collectors (ISCC plant)
549 was developed. The results obtained from the simulations were compared with the results
550 obtained from simulations of the combined cycle plant alone. Simulations for both cases were
551 performed first with 10% support from a steam flow from the solar plant and then with 20%
552 solar support. In both cases, the results were compared with the values obtained for the
553 combined cycle plant. Among the main results obtained, it was observed that an increase in the
554 steam support from the solar plant diminishes the flow of fuel from the furnace. The flow of
555 heat delivered by the furnace to the superheater diminishes with an increase in the mass flow of
556 steam provided by the solar plant. The supervisory MPC strategy developed for the steam
557 pressure in the superheater allows for the optimization of the fuel flow in the auxiliary burner,

558 thereby allowing the same steam pressure obtained using a PI control strategy to be produced
559 with less fuel consumption for the same power demand. The results demonstrate that in general,
560 fuel consumption is lower under the supervisory MPC strategy. The greatest differences are
561 observed when there is a decrease in the power of the steam turbine and when there is an
562 increase in the power of the gas turbine. The developed simulator is suitable for the study and
563 design of control strategies, for determining the sizing of equipment and for the dynamic
564 optimization of ISCC plants. Further research will focus on multivariable MPC control
565 strategies for ISCC plants and an analysis of the robustness of the MPC controller.

566

567 **Acknowledgments**

568 This work was partially supported by the Solar Energy Research Center (SERC) through
569 CONICYT: FBO16 and CONICYT/FONDAP/15110019. CVP is grateful for the support
570 provided by CONICYT-Chile through a doctorate scholarship and to the University of La
571 Serena for study leave.

572

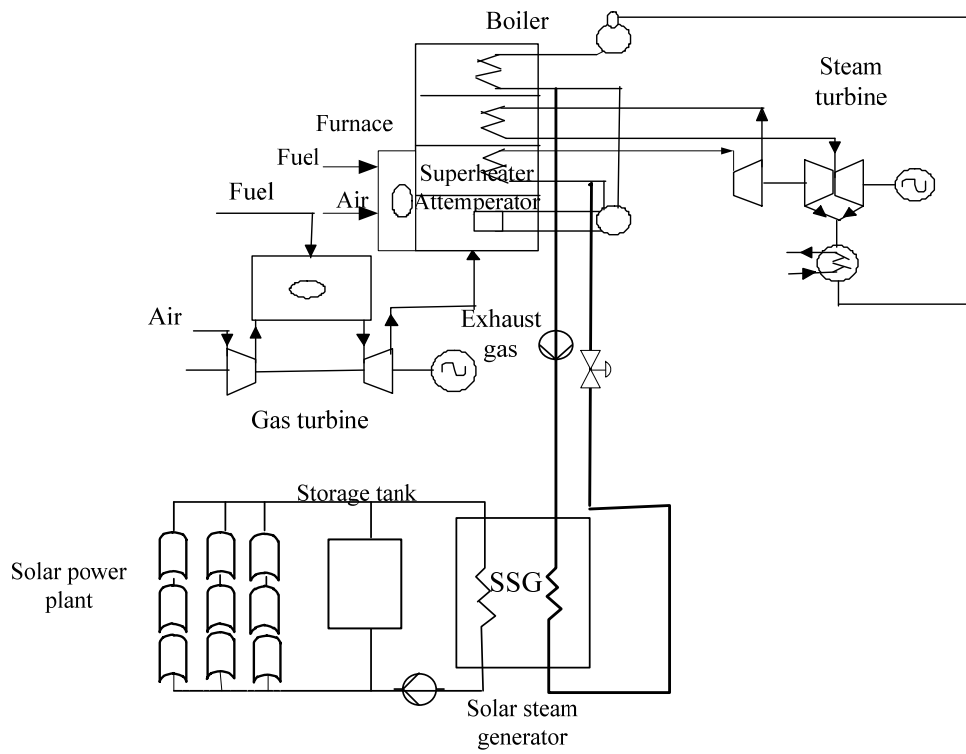
573 **References**

- 574 [1] Aftzoglou, Z., 2011. Exploring Integration Options in the Energy Sector, Including a Case Study of the
575 Integration of Solar Thermal Energy into a Combined Cycle Power Plant, MSc Thesis, Delft University of
576 Technology, Delft, The Netherlands.
- 577 [2] Amelio, M., Ferraro, V., Marinelli, V. and Summaria, A., 2014. An evaluation of the performance of an
578 integrated solar combined cycle plant provided with air-linear parabolic collectors. *Energy*, 69:742-748. DOI:
579 10.1016/j.energy.2014.03.068
- 580 [3] Al-Sulaiman, F. 2014. Exergy Analysis of Parabolic Trough Solar Collectors Integrated with Combined
581 Steam and Organic Rankine Cycle. *Energy Conversion and Management*, 77:441-449.
582 DOI:10.1016/j.enconman.2013.10.013
- 583 [4] Baghernejad, A. and Yaghoubi, M., 2010. Exergy Analysis of Integrated Solar Combined Cycle System.
584 *Renewable Energy*, 35(10): 2157-2164. DOI:10.1016/j.renene.2010.02.021
- 585 [5] Baghernejad, A. and Yaghoubi, M., 2011. Exergo-economic Analysis and Optimization of Integrated Solar
586 Combined Cycle System (ISCCS) Using Genetic Algorithm. *Energy Conversion and Management*, 52(5):
587 2193-2203. DOI: 10.1016/j.enconman.2010.12.019

- 588 [6] Behar, O., Kellaf, A., Mohamedi, K. and Belhamel, M., 2011. Instantaneous Performance of the First
589 Integrated Solar Combined Cycle System in Algeria. *Energy Procedia*, 6: 185-193. DOI:
590 10.1016/j.egypro.2011.05.022
- 591 [7] Behar, O., Kellaf, A., Mohammedi, K. and Ait-Kaci, S., 2014. A Review of Integrated Solar Combined
592 Cycle Systems (ISCCS) with a Parabolic Through Technology. *Renewable and Sustainable Energy Reviews*,
593 39: 223-250. DOI: 10.1016/j.rser.2014.07.066
- 594 [8] Camacho, E.F, Berenguel, M., and Rubio, F.R., 1993. Simulation Software Package of the Acurex Field,
595 E.S.I. of Sevilla, Internal Report, Sevilla.
- 596 [9] Camacho, E., Berenguel, M. and Rubio, M., 1997. *Advanced Control of Solar Plants*. Springer-Verlag,
597 London.
- 598 [10] Camacho, E.F., Berenguel Soria, M., Rubio, F.R., Martínez, D., 2012. *Control of Solar Energy Systems*.
599 Springer.
- 600 [11] Cau, G., Cocco, D. and Tola, V., 2012. Performance and Cost Assessment of Integrated Solar Combined
601 Cycle Systems (ISCCSs) Using CO₂ as Heat Transfer Fluid. *Solar Energy*, 86(10): 2975-2985. DOI:
602 10.1016/j.solener.2012.07.004
- 603 [12] Dersch, J., Geyer, M., Herrmann, U., Jones, S., Kelly, B., Kistner, R., Ortmanns, W., Pitz-Paal, R., and Price,
604 H., 2004. Trough Integration into Power Plants - a Study- on the Performance and Economy of Integrated
605 Solar Combined Cycle Systems. *Energy*, 29(5-6): 947-959. DOI: 10.1016/S0360-5442(03)00199-3
- 606 [13] Horn, M., Furing, H. and Rheinländer, J., 2004. Economic Analysis of Integrated Solar Combined Cycle
607 Power Plants: A Sample Case: The Economic Feasibility of an ISCCS Power Plant in Egypt. *Energy*, 29(5-
608 6): 935-945. DOI: 10.1016/S0360-5442(03)00198-1
- 609 [14] Hosseini, R., Soltani, M. and Valizadeh, G., 2005. Technical and Economic Assessment of the Integrated
610 Solar Combined Cycle Power Plants in Iran. *Renewable Energy*, 30(10): 1541-1555. DOI:
611 10.1016/j.renene.2004.11.005
- 612 [15] Kelly, B., Herrmann, U. and Hale, M.J., 2001. Optimization Studies for Integrated Solar Combined Cycle
613 Systems. *Proceeding of Solar Forum 2001, Solar Energy: The Power to Choose*, Washington DC, USA,
614 April 21-25 2001.
- 615 [16] Lambert, T., Hoadley, A. and Hooper, B., 2014. Process integration of solar thermal energy with natural gas
616 combined cycle carbon capture. *Energy*, 74:248-253. DOI: 10.1016/j.energy.2014.06.038
- 617 [17] Nezammahalleh, H., Farhadi, F. and Tanhaemami, M., 2010. Conceptual Design and Techno-economic
618 Assessment of Integrated Solar Combined Cycle System with DSG Technology. *Solar Energy*, 84(9): 1696-
619 1705. DOI: 10.1016/j.solener.2010.05.007
- 620 [18] Ordys, A., Pike, A., Johnson, M. and Katebi, R., 1994. *Modelling and Simulation of Power Generation*
621 *Plants*. Springer-Verlag, London.
- 622 [19] Price, H., Lüpfert, E., Kearny, D., Zarza, E., Cohen, G., Gee, R., Mahoney, R., 2002. Advances in Parabolic
623 Trough Solar Power Technology. *Journal of Solar Energy Engineering*, 124(2): 109-125. DOI:
624 10.1115/1.1467922
- 625 [20] Reid, R., Prausnitz, J. & Poling, B., 1987. *Properties of Gases and Liquids*. Nueva York: McGraw-Hill Co.
- 626 [21] Reynolds, W., 1979. *Thermodynamic Properties in SI*, USA: Mechanical Eng. Dept. Stanford University.
- 627 [22] Sáez, D., Cipriano, A. and Ordys, A., 2002. *Optimization of Industrial Processes at Supervisory Level*.
628 Application to Control of Thermal Power Plants. Springer-Verlag, London.
- 629 [23] Spelling, J., Favrat, D., Martin, A. and Augsburg, G., 2012. Thermoeconomic optimization of a combined-
630 cycle solar tower power plant. *Energy*, 41(1): 113-120. DOI: 10.1016/j.energy.2011.03.073

631
632
633
634

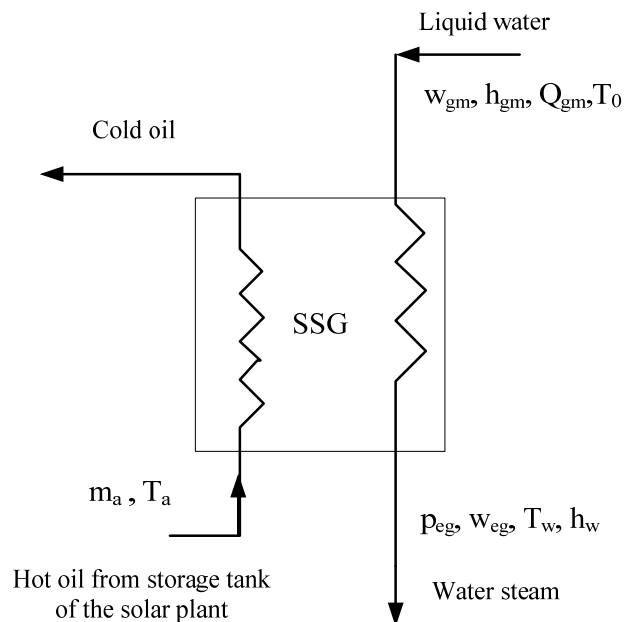
635 **Figures**



636

637

Fig. 1. ISCC diagram.

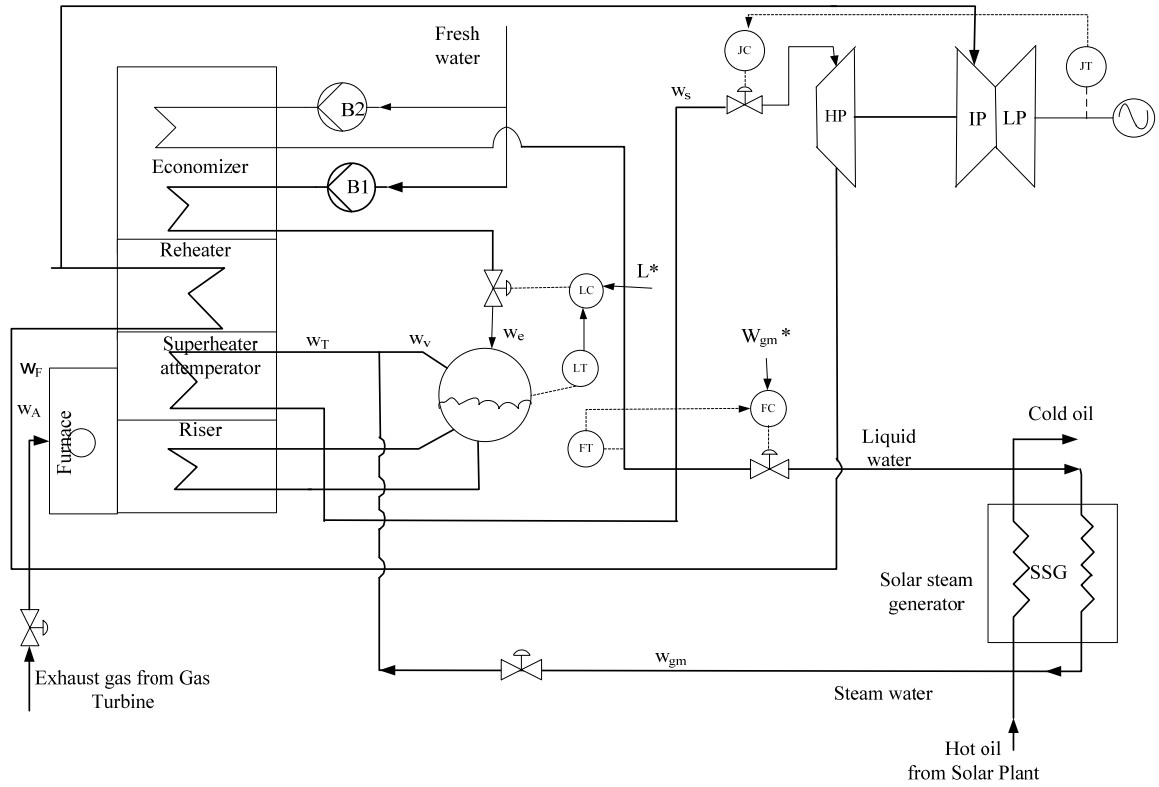


638

639

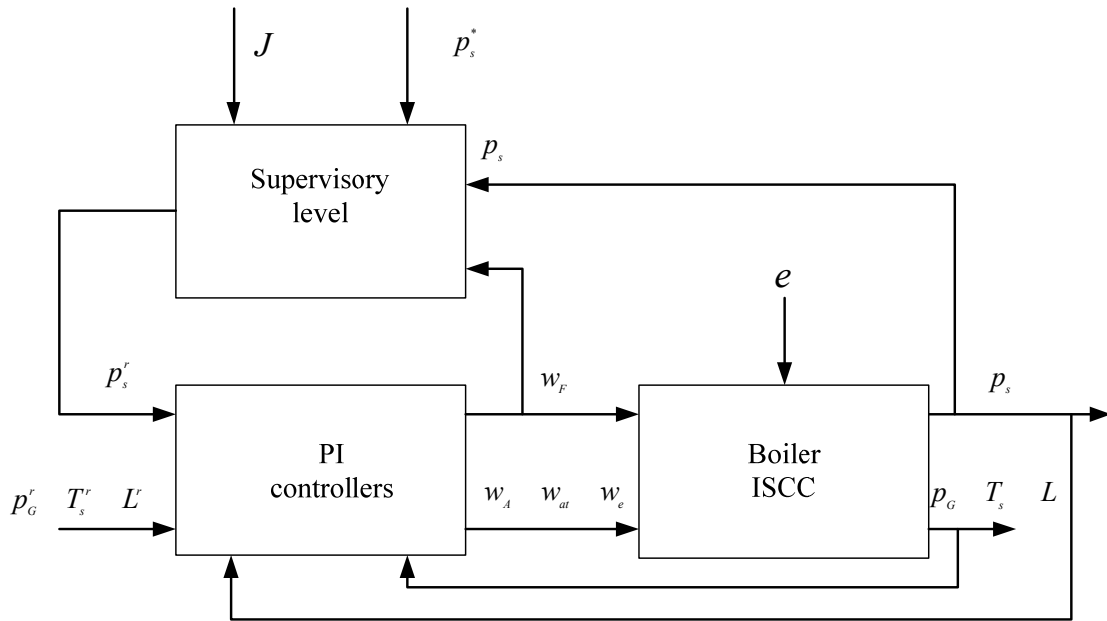
640

Fig. 2. Schematic diagram of the process of heat interchange from the hot oil originating from the solar plant to the steam water injected into the boiler.



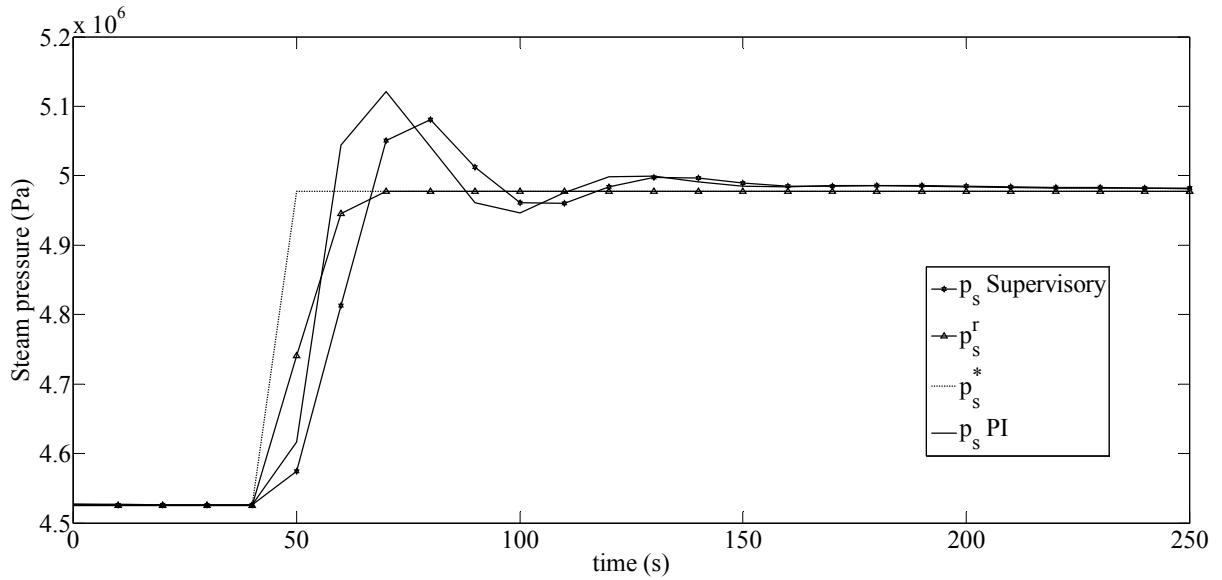
641
642
643

Fig. 3. SSG connected to a CC plant.



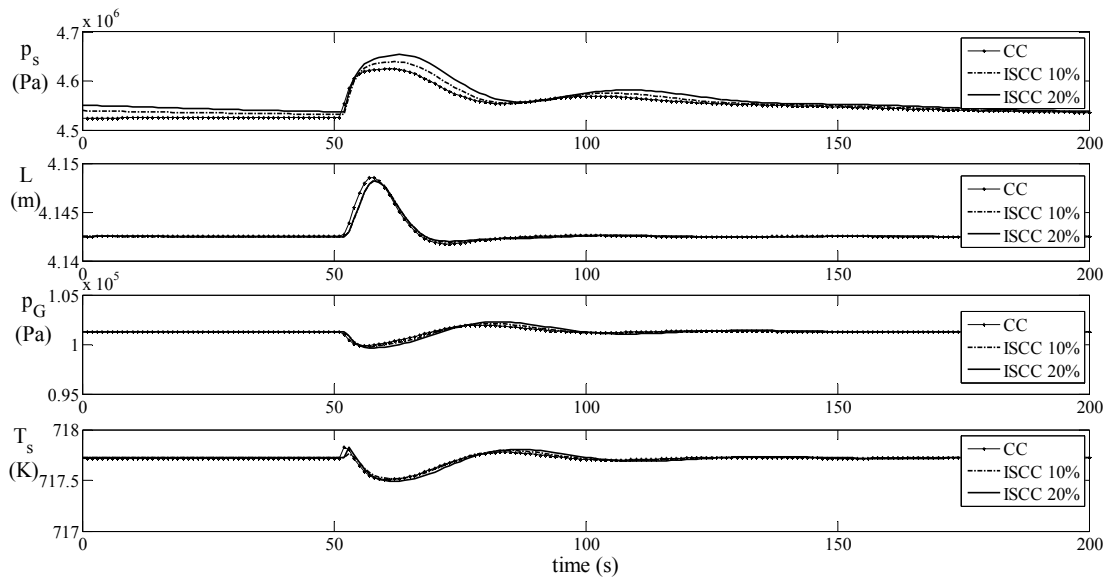
644
645

Fig. 4. Control scheme including supervisory level.



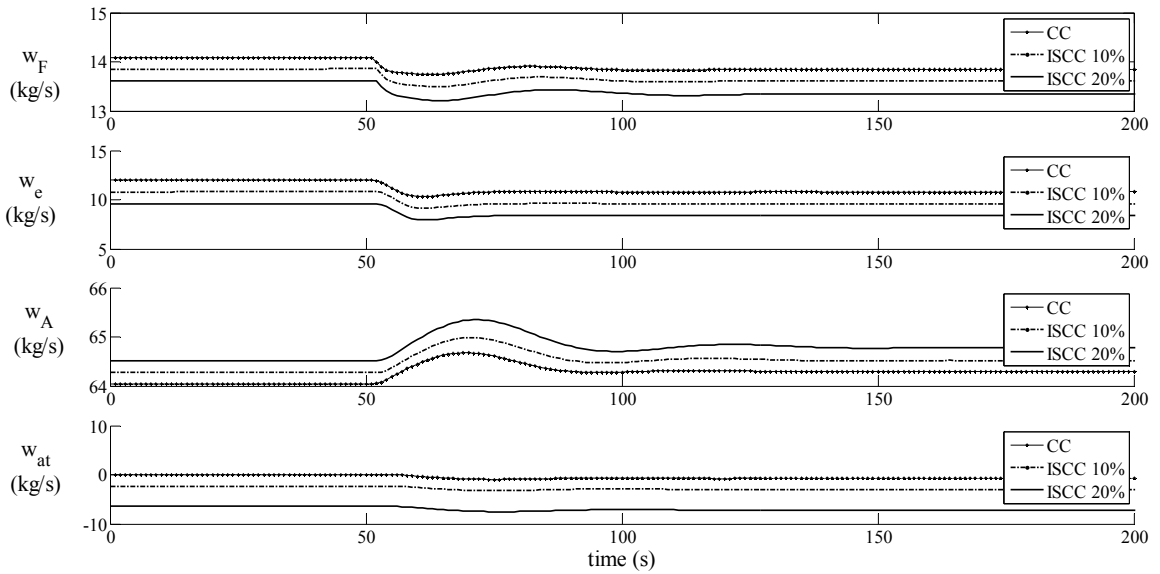
646
647
648
649

Fig. 5. Steam pressure response with a step-function change in the steam pressure set point at 50 s.



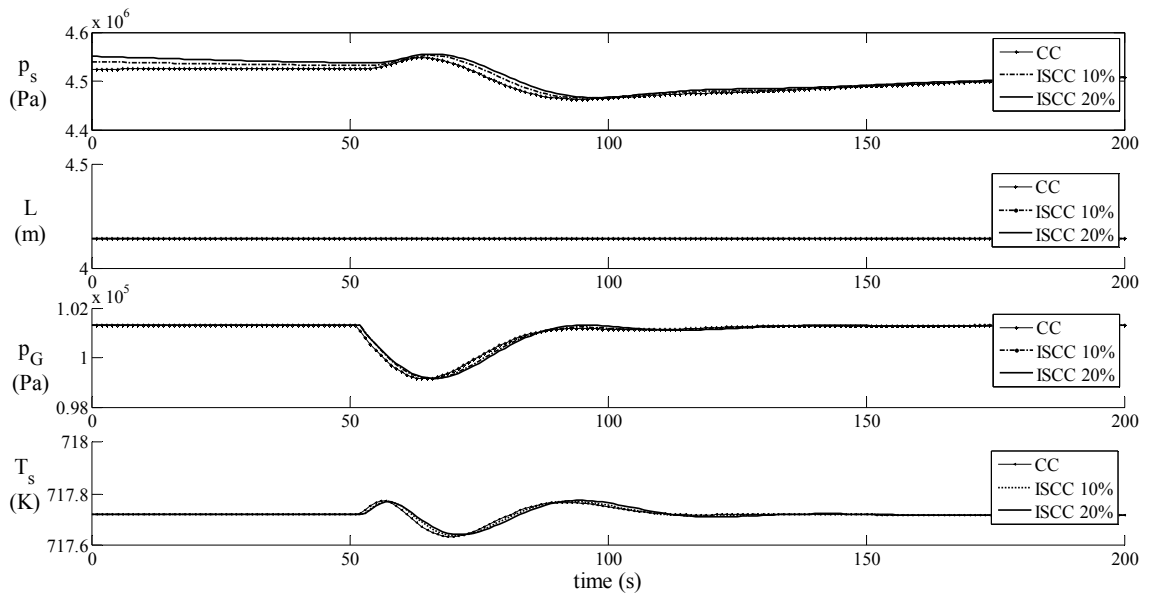
650
651
652

Fig. 6. Boiler response to a step-function change in the steam turbine power set point P_s^* (controlled variables).



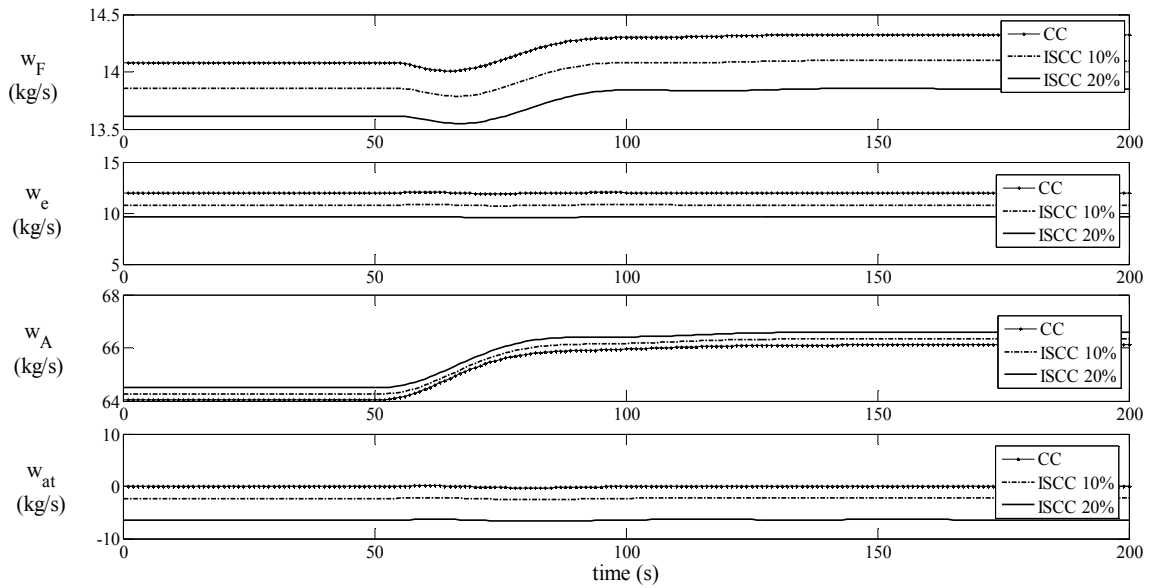
653
654
655

Fig. 7. Boiler response to a step-function change in the steam turbine power set point P_s^* (manipulated variables).



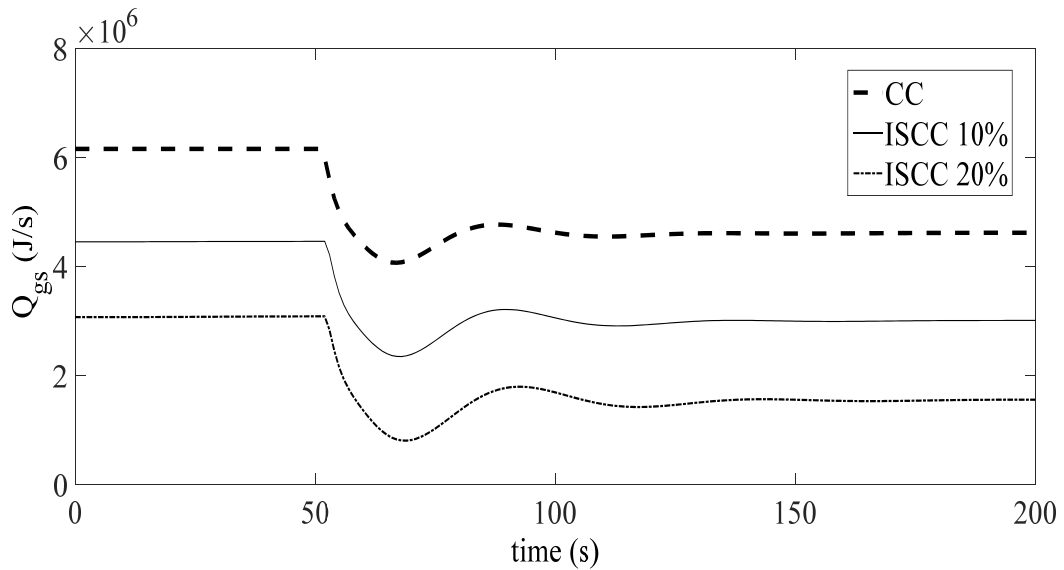
656
657
658

Fig. 8. Boiler response to a step-function change in the gas turbine power set point P_G^* (controlled variables).



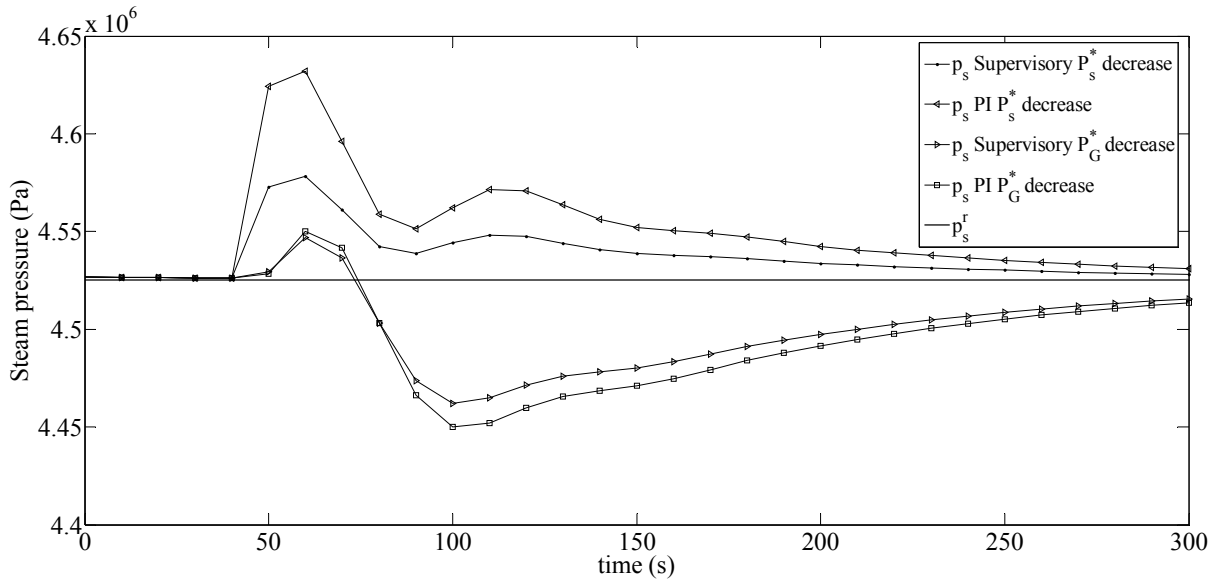
659
660
661
662

Fig. 9. Boiler response to a step-function change in the gas turbine power set point P_G^* (manipulated variables).



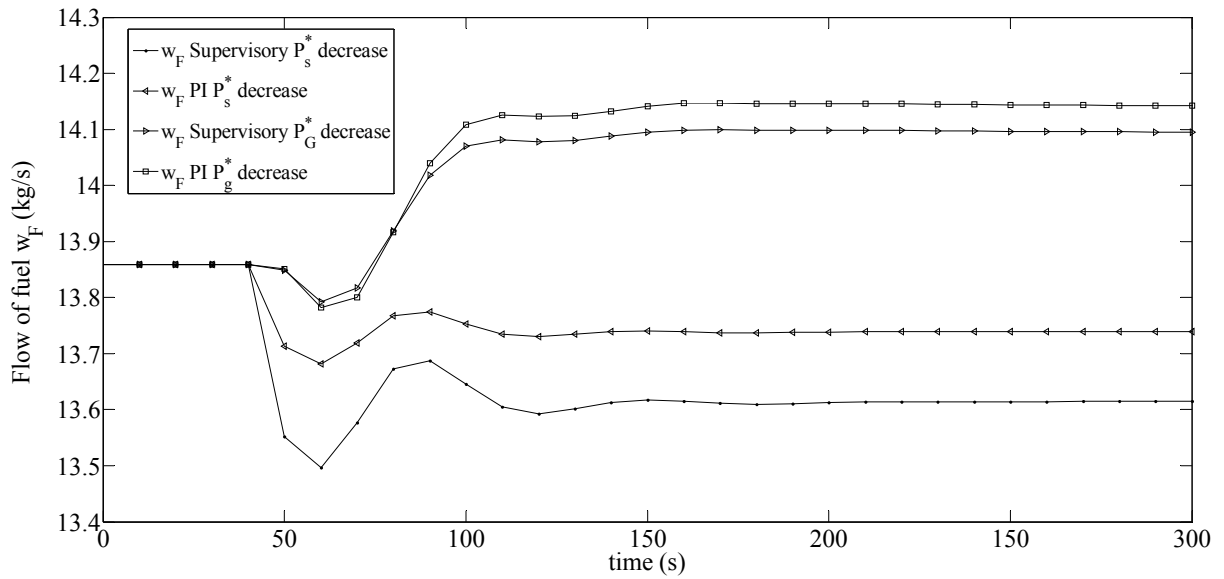
663
664
665
666
667

Fig. 10. Heat transferred to the superheater when the steam turbine power set point P_s^* is varied.



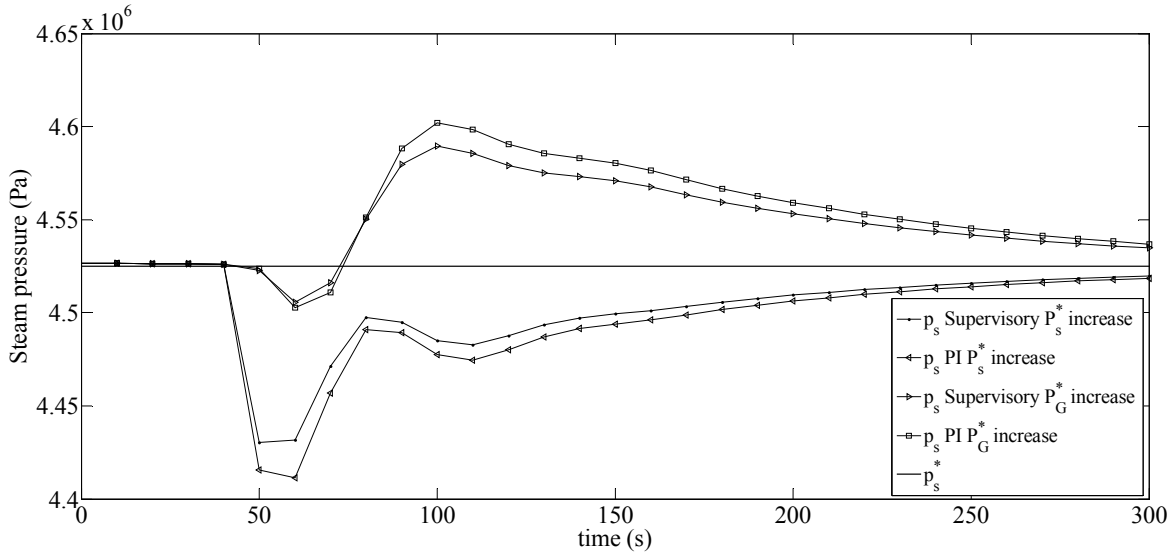
668
669
670
671

Fig. 11. Steam pressure responses to a step-function change (decrease) in the steam turbine power set point (P_s^*) and in the gas turbine power set point (P_G^*).



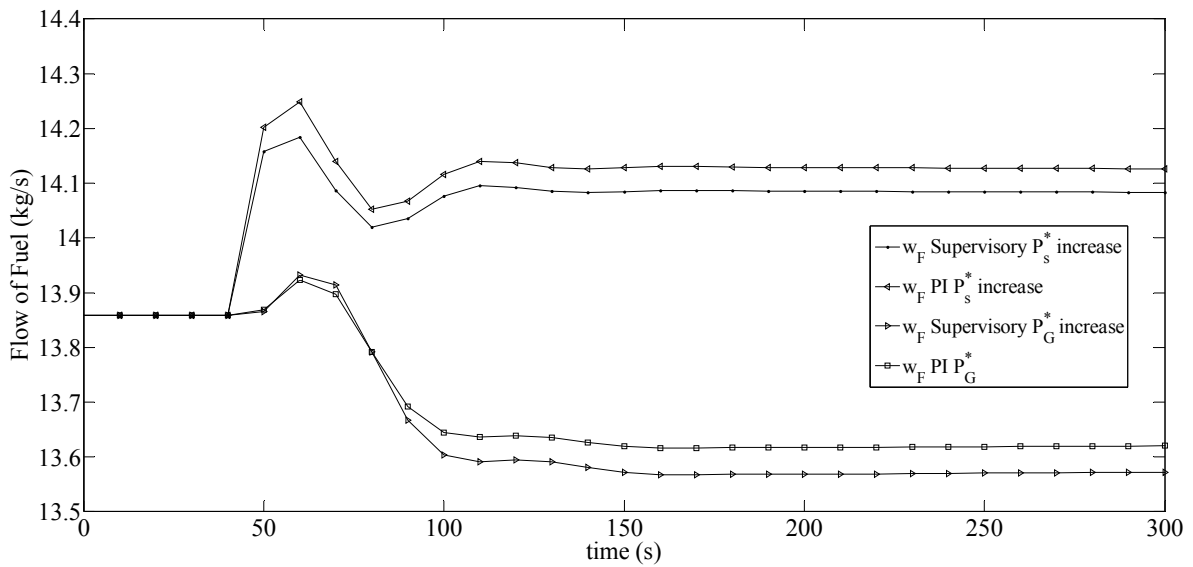
672
673
674
675

Fig. 12. Fuel flow responses, with PI and supervisory controllers, to a step-function change (decrease) in the steam turbine power set point (P_s^*) and in the gas turbine power set point (P_G^*).



676

677 Fig. 13. Steam pressure responses to a step-function change (increase) in the steam turbine
 678 power set point (P_s^*) and in the gas turbine power set point (P_G^*).
 679



680

681 Fig. 14. Fuel flow responses to a step-function change (increase) in the steam turbine power set
 682 point (P_s^*) and in the gas turbine power set point (P_G^*).
 683
 684

685 **Tables**

686 Table 1: Savings achieved using an ISCC plant.

	Fuel savings
10% SSG support	1.7%
20% SSG support	3.7%

687

688

Table 2: Evaluation index I_{wF}

	Supervisory MPC scheme	PI controller	ΔI_{wF}	Savings (%)
I_{wF} kg/s 10%	13.90	13.94	0.04	0.30
I_{wF} kg/s 15%	13.73	13.78	0.05	0.37
I_{wF} kg/s 20%	13.61	13.67	0.06	0.44

689

690

691 Table 3: Savings in fuel consumption between the supervisory MPC and PI control strategies.

	I_{wF} (kg/s), Supervisory MPC strategy	I_{wF} (kg/s), PI controller	ΔwF (kg)	Savings (%)
P_s^* (-)	13.61	13.74	0.13	0.92
P_s^* (+)	14.09	14.13	0.04	0.30
P_G^* (-)	14.10	14.14	0.05	0.33
P_G^* (+)	13.66	13.76	0.10	0.73

692